Spectral dependence of femtosecond laser induced circular optical properties in silica

Jing Tian,[1] Rubing Li,[2] Sang Hyuk Yoo,[3] Bertrand Poumellec,[1] Enric Garcia-Caurel,[3] Razvigor Ossikovski,[3] Michel Stchakovsky,[4] Celine Eypert,[4] John Canning,[5] and Matthieu Lancry[1,*]

[1]*Institut de Chimie Moléculaire et des Matériaux d'Orsay, UMR CNRS-UPS 8182, Université Paris Sud, Orsay, France*
[2]*Institute of Circular Economy, Beijing University of Technology, Beijing, 100124, China*
[3]*LPICM, CNRS, Ecole Polytechnique, Palaiseau, France*
[4]*HORIBA Europe Research Center, Palaiseau, France*
[5]*interdisciplinary Photonic Laboratories (iPL), University of Technology Sydney (UTS), NSW 2007, Sydney, Australia*
[*]*matthieu.lancry@u-psud.fr*

Abstract: Transmission Mueller-matrix spectroscopic ellipsometry is applied to study femtosecond laser induced nanogratings in silica glass in a wide spectral range 250–1800 nm. By using differential decomposition of the Mueller matrix, the circular birefringence and dichroism of femtosecond laser irradiated SiO_2 are quantified for the first time in the UV and near-IR range. A maximum value of the effective specific rotation of $\alpha \sim -860°/$mm at 290 nm is found. In the near-IR range, we found a linear and circular dichroism band peaking around 1240 nm, which might be attributed to the formation of anisotropic species like the formation of oriented OH species and Si-O-Si bond.

1. Introduction

Femtosecond laser direct writing (FLDW) starts with multiphoton ionization [1,2], which induces various permanent modifications in silica glass depending on the laser parameters [3], Such changes include refractive index changes [4], the formation of porous nanogratings and related linear birefringence [5–7], or even voids. The processing of glass with low-energy femtosecond laser pulses (sometimes combined with chemical etching) defines a flexible manufacturing platform suitable for technologies like optical data storage, optofluidics, optomechanics, marking, and photonics such as 3D optical waveguides and their combination [8,9], fiber Bragg gratings [10,11] and polarization devices [12,13]. Manufacturing monolithically integrated devices is attracting great interest because it is possible to induce strong refractive index increases (Δn from 10^{-3} to more than 10^{-2} in a large range of transparent glasses), which are localized in the bulk due to strong non-linear effect. Controlling these modifications could potentially allow exceeding current fs laser applications opening additional new possibilities in material science. In particular, the industrial demand for sophisticated all-optical integration is increasingly large as the volume of exchanged data and information increases demanding more complex devices and therefore greater nuance and complexity of laser treatment. Presently, one crucial optical property is still missing from the component library: the integration of circular optical properties (optical rotation and circular dichroism) in glass optical materials and devices.

In a previous study done in 2008, based on measurements done with a phase shift interferometer, we revealed that femtosecond laser interactions can shear matter like a scissor giving rise to a chiral strain if the light propagation axis is considered [14,15]. But shearing does not give rise to optical circular properties by itself like it is with torsion. Taylor *et al.* reported highly ordered «

chiral-like » nanostructures using circular polarized laser light but no circular optical properties [16]. In this direction, we have shown in 2016 that it is possible to produce circular diattenuation by inducing and controlling chirality within an achiral glass namely SiO_2 by controlling the laser writing polarization with respect to the scanning direction [17]. Last estimates of equivalent circular diattenuation using a circular dichroism spectrophotometer [18,19] show values up to $-30°$/mm in the UV wavelength range and $-20°$/mm at $\lambda = 550$ nm. However it was difficult to extract the real spectral shape of the circular diattenuation due to the co-existence of strong linear properties [19].
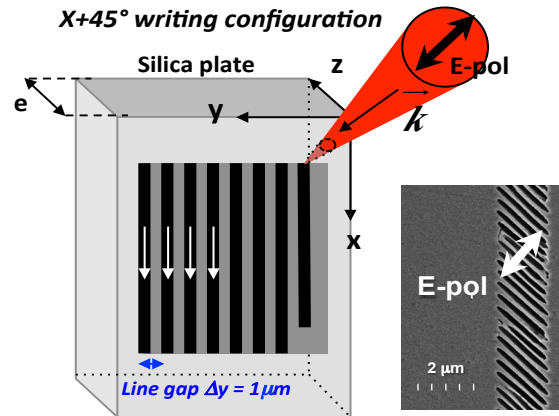
Recently Mueller-matrix spectroscopic ellipsometry was used in the visible range to investigated silica glass modified by femtosecond laser within nanogratings regime [20,21]. This method is a powerful tool to examine structural and optical properties of surfaces, thin films, and multilayered materials that exhibit both linear and circular optical properties from a single measurement. We applied the differential matrix formalism [22,23] on transmission Mueller matrices measured for femtosecond laser-induced modifications in silica within the type II laser-processing regime. We showed how values of the effective structural circular birefringence can be extracted in the presence of strong linear optical properties and found a maximum value of the effective specific rotation $\alpha \sim -143°$/mm at 550 nm.

In this letter, the spectral dependence of both linear and circular optical properties are investigated according to pulse energy and in a wide spectral range extending from $\lambda = 250$ nm up to $\lambda = 1800$ nm. In particular, we reveal a large effective optical rotation in the UV range and a specific dichroism band in the near-IR range when the laser polarization is oriented at 45° off the scanning direction.

2. Experimental details

The laser radiation was produced by a femtosecond laser system operating at $\lambda = 1030$ nm and delivering 250 fs pulses at 100 kHz repetition rate. The beam was focused to a depth 300 µm below the front face of 1 mm thick silica glass plates (Heraeus Suprasil1 containing [OH] $\sim$ 830 ppm and a solgel silica with [OH] $\sim$ 100 ppm) using a 0.6 NA aspheric lens (estimated beam waist $w \sim 1,5$ µm). The laser energy was varied from 0,15µJ up to 4µJ so we crossed the type II threshold (typ. 0,3µJ in our experimental conditions) corresponding to the formation of nanogratings in SiO_2. Based on preliminary results, we choose to investigate here a specific writing configuration in terms of polarization orientation that maximizes the imprinting of circular optical properties. When the laser was moving along x-axis (horizontal direction) and the laser linear polarization was oriented $\theta = +45°$ from the writing direction, we define it as "X + 45°" configuration of writing. Then, in this X + 45° configuration and using a scanning speed of $v = 1$ mm/s, we created several squares 3×3 mm^2, made up of a set of lines with a line spacing $\Delta y = 1$ µm to have a uniform anisotropic area and avoiding any diffraction effects. Scheme about the laser writing procedure is shown in Fig. 1 and more details can be found in Ref. [17].

Anisotropic optical properties are investigated using a phase modulated spectroscopic ellipsometer (UVISEL+, HORIBA Scientific) over $\lambda = 250$ to 1800 nm spectral range. Since this equipment gives access to the three first columns of the Mueller matrix [24], we will explain in the results section how to estimate the values of the 4th column based on symmetry properties of Mueller matrices. In order to validate this approach, we compared the data obtained with the UVISEL+ with data obtained with a home-made Mueller ellipsometer [24,25] (Smart-SE, HORIBA Scientific), which provides a full Mueller matrix over a shorter spectral range between $\lambda = 450$ and $\lambda = 1000$ nm. All measurements were made using a collimated probe beam in normal incidence. The probe beam size of these two instruments was fixed to 1 mm for all measurements. The samples were oriented in such a way their writing/scanning axis was set horizontal +/− 2° for the referential of the Mueller ellipsometers.
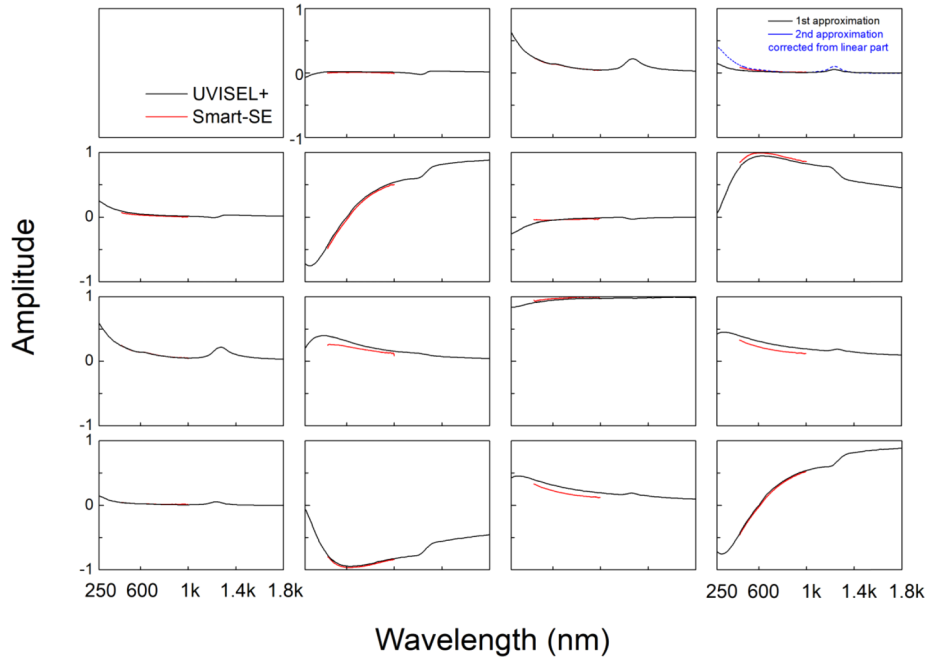
Fig. 1. Experimental setup scheme for X + 45° writing configuration and SEM image of sub-wavelength periodic structure formed in cross-section of the irradiated region. Original image is courtesy of Dr. Cyril Hnatovsky.

3. Results

We have seen in our preliminary experiments that our samples show asymmetric transmission when measuring ellipticity using a circular dichroism spectrometer [19]. In 2018 we investigated this observation by measuring both $\mathbf{M}$ and $\mathbf{M_{rev}}$, i.e., the Mueller matrix in the reverse direction (from the backface) [21]. The differences were that m_{13}, m_{31}, m_{24}, and m_{42} change their respective signs whereas all other elements remain invariant. This symmetry implies that $\mathbf{M}$ fulfills the principle of reciprocity. The difference between the elements of predicted $\mathbf{M_{rev}}$ from a measured Mueller matrix, $\mathbf{M}$, and the elements of the measured $\mathbf{M_{rev}}$ is typically < 0.01 which corresponds to instruments accuracy. This indicates that both linear and circular anisotropic optical properties are quite similarly distributed in depth.

Figure 2 shows the normalized (m_{11} was normalized to 1) spectral Mueller matrices M obtained with the two instruments. The Mueller matrix represented in this figure corresponds to a Suprasil1 sample written at pulse $E = 1.5$ µJ/pulse with a X + 45° writing configuration. The sample exhibits low linear and circular dichroism because the elements m_{12}, m_{21}, m_{14} and m_{41} are very small. In contrast, the elements m_{24} and m_{42}, being close to $+ 1$ and $−1$ respectively highlight a significantly high linear birefringence [26]. The Mueller matrix of this "X + 45°" sample, can be firstly approximated by $\mathbf{M} = \mathbf{R(−45°)}.\mathbf{M_{\Psi\Delta}}.\mathbf{R(45°)}$, where $\mathbf{R(\alpha)}$ is the rotation matrix and $\mathbf{M_{\Psi\Delta}}$ is the Mueller matrix for a perfect linear dichroic retarder. This corresponds to the slow axis direction coinciding with the chosen writing polarization orientation; that is, rotated $\alpha = 45°$ from the direction of writing. The element m_{33} should ideally be equal to one. However, the measured values appear to be slightly smaller (0.95–0.99) indicating a slight depolarization, and down to 0.85 in the UV range at $\lambda = 250$ nm. In summary, our samples for $\lambda \in 450$–1800 nm are characterized by having high linear retardation, low dichroism, and a small depolarization. Note there is an interesting dichroic band around $\lambda = 1300$ nm. In the UV range, there is an increase of the linear dichroism and a significant depolarization.

So as a first approximation if we consider that our sample is indeed a linear dichroic retarder at 45° (i.e. circular properties are very small compared to the linear ones), we can use symmetry properties of Mueller matrices to evaluate the values of the 4th column i.e. $m_{14} = m_{41}$, $m_{24} = −m_{42}$, $m_{34} = m_{43}$, $m_{44} = m_{22}$. Note that both matrices coincide quite well in the common spectral range so this first approximation to deduce the values of the 4th column of the Mueller matrix from phase-modulated ellipsometry could provide some reliable information. Note that the differences
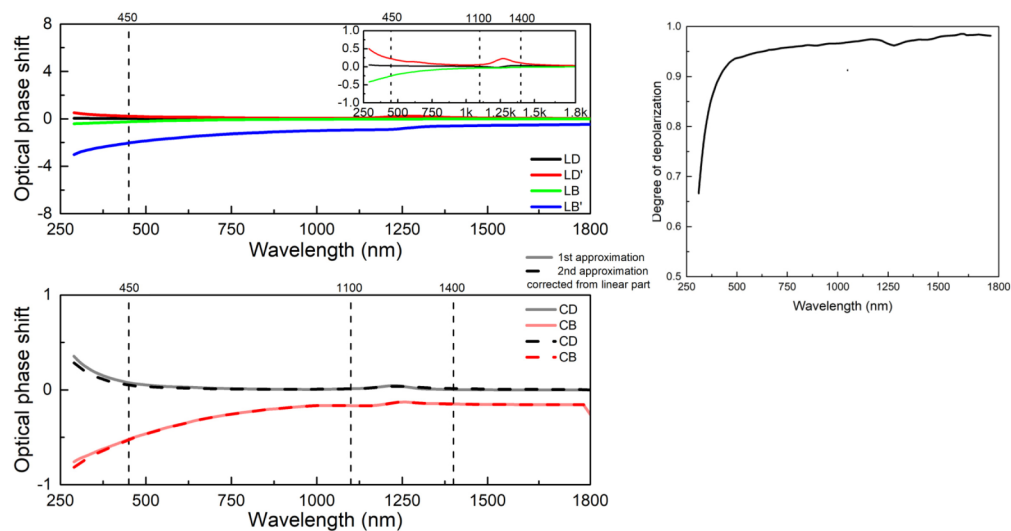
Fig. 2. Normalized Mueller matrix of Suprasil1 written using X + 45° configuration. Red lines are for the liquid crystals ellipsometer whereas the one obtained with photoelastic modulator ellipsometer correspond to the black lines. The dash blue line corresponds to the second order approximation taking into account the linear contribution

between the two ellipsometers (e.g. up to 0,1 in m_{32} and m_{34}) are related to a slightly different azimuthal orientation (+/−2°) of the samples during measurements. This leads to different "projections" of the linear properties in the xy plan but this has no impact on the intrinsic polarimetric properties that we extract after decomposition.

As a second order approximation we can take into account that elements m_{14} and m_{41} is formed by a superposition of effects due to both circular and linear parts, with the linear contribution intervening with opposite signs in m_{14} and m_{41} respectively as it has been extensively study in Refs. [27–29]. Therefore since linear properties are non-zero, one expects that before decomposition m_{14} be different than m_{41}. So the dash blue line in Fig. 2 corresponds to m_{14} taking into account the linear, which agree quite well with the full Mueller ellipsometer (Smart-SE). This enables further data treatment in order to determine the complete polarimetric properties of our fs-irradiated samples.

According to [23] the polarimetric optical response of a medium of length, l, with a complex refractive index $\tilde{n} = n + i.\kappa$, can be defined as a superposition of the following optical phase shift related to basic polarimetric properties: linear birefringence $LB = \frac{2\pi}{\lambda}.(n_X - n_Y).l$, 45° linear birefringence $LB' = \frac{2\pi}{\lambda}.(n_{45} - n_{135}).l$, linear dichroism $LD = \frac{2\pi}{\lambda}.(\kappa_X - \kappa_Y).l$, 45° linear dichroism $LD' = \frac{2\pi}{\lambda}.(\kappa_{45} - \kappa_{135}).l$, circular birefringence $CB = \frac{2\pi}{\lambda}.(n_L - n_R).$, circular dichroism $CD = \frac{2\pi}{\lambda}.(\kappa_L - \kappa_R).l$ and the degree of polarization DoP. By using the differential decomposition described in [5–6], it is possible to extract all the above mentioned polarimetric properties from the Mueller matrix of a sample providing that the laser track is considered as homogeneous in the direction of light propagation. A differential decomposition of **M** to find its differential matrix, **m**, implies determining its logarithm $\mathbf{L} = \ln(\mathbf{M})$. Since $d\mathbf{M}/dz = \mathbf{m}(z).\mathbf{M}(z)$, if the differential matrix **m**, does not depend on z, then the matrices **m** and **L** are related by $\mathbf{L} = \mathbf{m}.l$. For a

non-depolarizing medium, the differential matrix **L** is Minkowski antisymmetric and contains the six elementary optical properties fully characterizing the medium namely *LD, LB, LD', LB', CD, CB* and the *DoP*. When the medium is depolarizing as it is the case here in the UV range (DoP decreases down to 0,7 at $\lambda = 300$ nm as shown in the right inset of Fig. 3), the depolarization can be interpreted as resulting from the fluctuations of the optical properties n and κ, which influence the elementary polarization properties of the irradiated silica glass [22,23]. Result of the differential decomposition of the experimental Mueller matrix is shown in Fig. 3. Based on preliminary investigations [17,19] we know that fs-irradiation modifies inhomogeneously the physical structure of the material along the pulse path across the sample. Consequently, we think that the measured birefringence parameters do not correspond to intrinsic material properties but to effective or equivalent optical parameters induced by fs laser. For sake of comparison we add the *CB* and *CD* spectra obtained from the decomposition of the Mueller matrix using the two different approximations describe above: first one (full line) considers circular properties are very small when compared to the linear ones whereas the second one (dash line) introduce a linear term correction to calculate the elements of 4th column as described in [27–29].
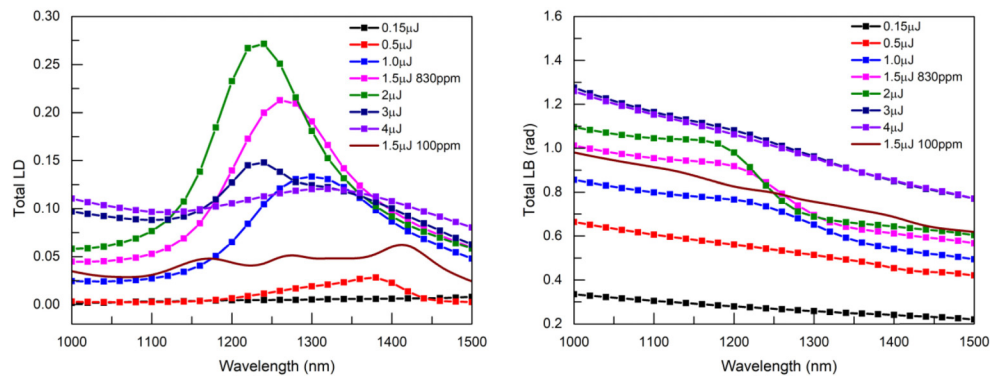

Fig. 3. Spectral dependence of the anisotropic linear and circular optical properties and extracted after Mueller matrix decomposition. (Suprasil1 silica, 1030 nm, 250 fs, 0.6 NA, 1 mm/s, 100kHz, 1,5µJ/pulse, X + 45° configuration). The dashed lines correspond to data decomposed using the second order approximation taking into account the linear contribution. The right inset corresponds to the Degree of Polarization (DoP) spectral dependence.

We can observe three spectral regions in Fig. 3: (I) below $\lambda = 450$ nm, (II) $\Delta\lambda = (450–1100)$ nm and above $\lambda = 1400$ nm, and (III) between $\lambda = 1100$ and $\lambda = 1400$ nm. In region I, the absolute values of the off-diagonal elements in M are quite high which have values above 0.3 rad. For example, at $\lambda = 250$ nm, we reveal 0.5 for *LD'*, -3 rad for *LB'* and significant circular properties as well 0.3 *CD* for and -0.75 rad for *CB*. Note that the reliable presence of *CD* in the UV range has previously been confirmed using a spectro-polarimeter in [18]. In region II, all depolarization effects remain smaller than 10% and monotonically decrease with λ below 3% for $\lambda > 1100$ nm. According to the data shown in Fig. 3, it is seen that the two *xy* linear effects (*LB* and *LD*) are small, while the crossed linear properties (*LB'* and *LD'*) are quite important. This is because the polarization of the sample (X + 45°) written by laser was oriented ± 45° to the reference axis. If the polarization had been oriented parallel or perpendicular to the x-direction (X0° or X90°), the pair (*LB* and *LD*) would have been maximal and the pair (*LD'* and *LB'*) would have been
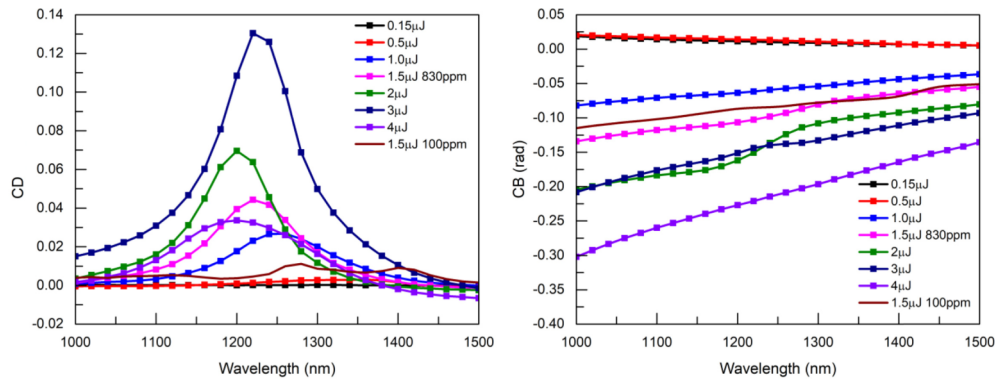
minimized. For the circular effects we notice a monotonous increase of *CD* towards shorter wavelengths.

In region III $\Delta\lambda = (1100 - 1400)$ nm, the sample exhibits a strong linear dichroism at 45° (*LD'*) band. In particular we notice that $m_{13} \approx m_{31}$ with *LD'* values up to 0.25. For the chosen orientation we also observe that $m_{14} \approx m_{41}$ and is nonzero with *CD* values up to 0.10, which reveals a slight circular dichroic band. The corresponding Kramers–Kronig consistent feature in *LB'* and *CB* also creates a related feature $\sim \lambda = 1240$ nm.

The spectral dependence of both linear and circular anisotropic optical properties are shown respectively in Figs. 4 and 5 as a function of the pulse energy. In Fig. 4 we chose to draw the "*Total LB*" and the "*Total LD*" that correspond to the following equations *Total LB* $= \sqrt{LB^2 + LB'^2}$ and *Total LD* $= \sqrt{LD^2 + LD'^2}$. Note that these two properties are thus independent of the samples azimuthal orientation during the ellipsometry measurements.

Fig. 4. Near-IR spectral dependence of the total linear birefringence, LB (Left), and the total linear dichroism, LD (Right), as a function of fs pulse energy. (1030 nm, 250 fs, 0.6 NA, 1 mm/s, 100 kHz, X + 45° configuration). Dots are for Suprasil1 silica whereas full line is for 100 ppm OH sample.

Fig. 5. Near-IR spectral dependence of circular birefringence, CB (Left), and circular dichroism, CD (Right), (expressed in radians) as a function of femtosecond laser pulse energy (1030 nm, 250 fs, 0.6 NA, 1 mm/s, 100 kHz, X + 45° configuration). Dots are for Suprasil1 silica (830 ppm OH) whereas full brown line is for 100 ppm OH silica sample.

Below 1100 nm, the amplitudes of the anisotropic linear properties are increasing monotonously with increasing pulse energy, *E*, from 0.15 µJ up to 4 µJ. Above 0.5 µJ, we can observe a linear

dichroism band within $\Delta\lambda = (1100–1400)$ nm as revealed in Fig. 4(Left). The amplitude of this *LD* band increases with the energy of the fs pulse and the sample shows a maximum *LD* of 0.27 rad at $\Delta\lambda = 1240$ nm for $E = 2$ μJ. The spectral position of the band also shifts from 1380 nm at $E = 0.5$ μJ down to 1240 nm at 2 μJ. This agrees with the corresponding Kramers–Kronig-consistent feature in the LB spectra that creates an increasing spectral feature around $\Delta\lambda \sim 1240$ nm up to 2 μJ as shown in Fig. 4(Right). However above 3 μJ, we observe a decrease of the *LD* amplitude and the band shifts back to longer wavelengths. Now comparing the two OH samples written with $E = 1,5$ μJ, we can see that the « background *LB* » (away from the dichroic band e.g. around 1000 nm) did not almost change irrespectively of the OH species concentration in agreement with [30]. In contrast the amplitude of *LD* band(s) around 1100–1400 nm is much lower in the "low OH" sample (100 ppm, full brown line). It is worth noting that the dichroic band appears to be composed of 2 or even 3 unknown contributions that still remain to be identified.

The corresponding spectra related to the circular optical properties are shown in Fig. 5. Similar to the linear properties, we observed a *CD* band in the 1100–1400 nm spectral range, which evolves in the same way (increasing amplitude and blue shift) as the *LD* band according to the pulse energy up to 2 μJ. It is worth noting that the *CD* amplitude in the near IR is much lower (by a factor 5) in the "low OH" sample. In addition the *CB* spectra are consistent with Kramers–Kronig and a related feature that can be seen in Fig. 5(Right) around $\lambda \sim 1250$ nm, especially up to $E = 2$-3 μJ. Then from 3 μJ, the dependence is more complex since the *LD* amplitude is decreasing whereas *CD* band in Fig. 5(Left) is strongly increasing. This indicates that *CD* and *LD* amplitudes are not simply connected to each other. Following the same trend, *CD* and *CB* are no more Kramers–Kronig consistent for $E = 3$ μJ. This suggests that the origin of the circular properties is likely not related to chiral molecular species but rather to a chiral arrangement of anisotropic linear layers along the probe beam pathway. In the later case, a non-parallel non-orthogonal assembly of two *LB* (or *LD*) contributions would create some effective *CB* (respectively *CD*) whose amplitude is proportional to the *LB* (or *LD*) and the misalignment angle between the two contributions [31].

4. Discussion

Apart from the spectral feature around $\lambda \sim 1250$ nm, the linear optical properties are mainly related to the formation of nanogratings resulting in a strong linear form birefringence. However, there is also a slight contribution of stress-induced birefringence, which has been investigated in the literature [32,33]. We reported earlier that the spectral dependence of the optical pathway difference expressed as $(n_X - n_Y).l$ is quite flat in the investigated spectral range, which results in an increase of $LB = \frac{2\pi}{\lambda}.(n_X - n_Y).l$ at short wavelengths. An increasing apparent *LD* at short wavelength accompanies the linear birefringence, which is related to the nanogratings. The positive *LD'* (and nearly zero *LD*) observed in Fig. 3 implies that a higher losses were measured for polarization oriented perpendicular to the nanolayers in agreement with [34]. It is known that a layered medium made of alternating layers of two different isotropic materials with complex refractive indices, exhibits a linear dichroism [35]. However the linear dichroism observed in the UV-Vis range should be rather called linear diattenuation since it can be mostly attributed to polarization dependent scattering [34] due to the intrinsic nanoporous nature of the nanogratings.

About the observed circular optical properties in the UV-Vis range, we do not know yet if the observed circular birefringence originates from internal linear birefringence that could be related to a non-parallel non-orthogonal assembly of two (or more) linear contributions, or from a fs pulse induced molecular optical activity. However, we may, from the observed structural circular birefringence, estimate the value of an effective specific rotation; i.e. circular birefringence per unit length to facilitate comparison with naturally optically active materials. From Fig. 3, we find that *CB* at $\lambda = 290$ nm has an extreme value of -0.75 rad produced by the birefringent laser track

that exhibit a length of $l = 50$ μm (in the z-propagation direction). Therefore the specific rotation is $\frac{CB.180}{2\pi.l} \approx -860°$/mm.

Following the same view in the Near-IR range, we can deduce from Fig. 5 a maximum *CB* of -0.22 rad at 1240 nm for 4 μJ/pulse corresponding to an equivalent specific rotation estimated to $-126°$/mm. This could be compared with the specific rotation of natural materials, like quartz (less than 5°/mm at 1240 nm and 49°/mm at 400 nm) or the structural rotary power of liquid crystals (cholesteric monocrystalline layer can reach thousands of °/mm) [36]. Within this specific wavelength range, we can observe an intense dichroism band both linear and circular.

These bands might be related to vibrational absorption bands ascribed to the combination of $2.\nu_{stretching}$Si-OH + $\nu_{stretching}$Si-O-Si. Another possibility would be the combination $2.\nu_{stretching}$Si-OH + $\nu_{bending}$Si-OH [37]. Note there are some variants Si-OH silanol groups as described in [38], which could explain the occurrence of 2-3 bands as observed in the "low OH" sample. However there is no *CD* band at 1400 nm corresponding to the first harmonic of SiOH stretching, $2.\nu$OH, which indicates that *CD* origin might be related to Si-O-Si bonds arrangement. This was tentatively interpreted through the breaking of symmetry arising from a volume torque $\vec{P} \wedge \vec{E}_{DC}$ due to the combined action of the stress field and a DC electric field (defined by the pulse front tilt, the focusing conditions and the laser polarization). This volumetric torque may contribute to twist local matter and create chiral atomic arrangements [17]. However, it is unlikely that this could create a high enough population of Si-O-Si bonds with a chiral arrangement (such as tetrahedra in α-quartz) to achieve the observed high *CD*. Another possibility would be that *CD* band originates from several internal linear dichroism and birefringence contributions with non-parallel neutral axes. Following this view, the amplitude of the observed *CD* band is not only related to the *LD* or *LB* optical phase shift of each contribution but also to the misalignment between their neutral axes. Note that the *LB* neutral axis is mainly related to the form birefringence of the nanogratings.

5. Conclusion

We have investigated the polarimetric properties of femtosecond laser induced nanogratings in a wide spectral range extending from UV up to the NIR. The equivalent circular optical properties using Mueller-matrix spectroscopic ellipsometry in transmission mode were extracted. A high effective specific rotation of $\alpha \sim -860°$/mm at $\lambda = 290$ nm is found. We also reveal the formation of a linear and circular dichroism band peaking around $\lambda \sim 1240$ nm.

Funding

References

1. P. B. Corkum, "Plasma perspective on strong field multiphoton ionization," Phys. Rev. Lett. **71**(13), 1994–1997 (1993).
2. A. Couairon and A. Mysyrowicz, "Femtosecond filamentation in transparent media," Phys. Rep. **441**(2-4), 47–189 (2007).
3. B. Poumellec, M. Lancry, A. Chahid-Erraji, and P. Kazansky, "Modification thresholds in femtosecond laser processing of pure silica: review of dependencies on laser parameters [Invited]," Opt. Mater. Express **1**(4), 766–782 (2011).
4. K. Davis, K. Miura, N. Sugimoto, and K. Hirao, "Writing waveguides in glass with a femtosecond laser," Opt. Lett. **21**(21), 1729–1731 (1996).
5. M. Lancry, B. Poumellec, J. Canning, K. Cook, J. Ä. Poulin, and F. Brisset, "Ultrafast nanoporous silica formation driven by femtosecond laser irradiation," Laser Photon. Rev. **7**(6), 953–962 (2013).
6. S. Richter, A. Plech, M. Steinert, M. Heinrich, S. Doering, F. Zimmermann, U. Peschel, E. B. Kley, A. Tunnermann, and S. Nolte, "On the fundamental structure of femtosecond laser-induced nanogratings," Laser Photon. Rev. **6**(6), 787–792 (2012).

7. Y. Shimotsuma, P. Kazansky, J. Qiu, and K. Hirao, "Self-organized nanogratings in glass irradiated by ultrashort light pulses," Phys. Rev. Lett. **91**(24), 247405 (2003).

8. H. Zhang, S. Eaton, and P. Herman, "Low-loss Type II waveguide writing in fused silica with single picosecond laser pulses," Opt. Express **14**(11), 4826–4834 (2006).

9. S. M. Eaton, M. L. Ng, R. Osellame, and P. R. Herman, "High refractive index contrast in fused silica waveguides by tightly focused, high-repetition rate femtosecond laser," J. Non-Cryst. Solids **357**(11-13), 2387–2391 (2011).

10. G. Marshall and M. Withford, "Rapid Production of Arbitrary Fiber Bragg Gratings using Femtosecond Laser Radiation," Lasers and Electro-Optics Society, 2005. LEOS 2005. *The 18th Annual Meeting of the IEEE*, 935–936 (2005).

11. G. D. Marshall, R. J. Williams, N. Jovanovic, M. Steel, and M. J. Withford, "Point-by-point written fiber-Bragg gratings and their application in complex grating designs," Opt. Express **18**(19), 19844–19859 (2010).

12. M. Beresna, M. Gecevičius, and P. G. Kazansky, "Ultrafast laser direct writing and nanostructuring in transparent materials," Adv. Opt. Photon. **6**(3), 293–339 (2014).

13. M. Beresna, M. Gecevičius, and P. G. Kazansky, "Harnessing Ultrafast Laser Induced Nanostructures in Transparent Materials," in *Progress in Nonlinear Nano-Optics* (Springer, 2015), pp. 31–46.

14. B. Poumellec, M. Lancry, J. C. Poulin, and S. Ani-Joseph, "Non reciprocal writing and chirality in femtosecond laser irradiated silica," Opt. Express **16**(22), 18354–18361 (2008).

15. B. Poumellec, L. Sudrie, M. Franco, B. Prade, and A. Mysyrowicz, "Femtosecond laser irradiation stress induced in pure silica," Opt. Express **11**(9), 1070–1079 (2003).

16. R. Taylor, E. Simova, and C. Hnatovsky, "Creation of chiral structures inside fused silica glass," Opt. Lett. **33**(12), 1312–1314 (2008).

17. B. Poumellec, M. Lancry, R. Desmarchelier, E. Hervé, and B. Bourguignon, "Parity violation in chiral structure creation under femtosecond laser irradiation in silica glass?" Light: Sci. Appl. **5**(11), e16178 (2016).

18. J. Tian, R. Desmarchelier, B. Poumellec, and M. Lancry, "Femtosecond laser-induced circular dichroism in silica: Dependence on energy and focusing depth," Nucl. Instrum. Methods Phys. Res., Sect. B **435**, 258–262 (2018).

19. R. Desmarchelier, M. Lancry, J. Tian, and B. Poumellec, "Chiroptical properties photo-induced by femtosecond laser irradiation in silica glass," Appl. Phys. Lett. **110**(2), 021112 (2017).

20. Y. Shimotsuma, K. Miura, and H. Kazuyuki, "Nanomodification of Glass Using fs Laser," Int. J. Appl. Glass Sci. **4**(3), 182–191 (2013).

21. J. Tian, M. Lancry, S. H. Yoo, E. Garcia-Caurel, R. Ossikovski, and B. Poumellec, "Study of femtosecond laser-induced circular optical properties in silica by Mueller matrix spectropolarimetry," Opt. Lett. **42**(20), 4103–4106 (2017).

22. R. Ossikovski and O. Arteaga, "Statistical meaning of the differential Mueller matrix of depolarizing homogeneous media," Opt. Lett. **39**(15), 4470–4473 (2014).

23. R. Ossikovski, "Differential matrix formalism for depolarizing anisotropic media," Opt. Lett. **36**(12), 2330–2332 (2011).

24. E. Garcia-Caurel, A. De Martino, J.-P. Gaston, and L. Yan, "Application of spectroscopic ellipsometry and Mueller ellipsometry to optical characterization," Appl. Spectrosc. **67**(1), 1–21 (2013).

25. E. Garcia-Caurel, A. De Martino, and B. Drevillon, "Spectroscopic Mueller polarimeter based on liquid crystal devices," Thin Solid Films **455-456**, 120–123 (2004).

26. J. J. G. Perez and R. Ossikovski, *Polarized Light and the Mueller Matrix Approach* (CRC Press, 2016).

27. O. Arteaga and A. Canillas, "Pseudopolar decomposition of the Jones and Mueller-Jones exponential polarization matrices," J. Opt. Soc. Am. A **26**(4), 783–793 (2009).

28. O. Arteaga, Z. El-Hachemi, and A. Canillas, "Application of transmission ellipsometry to the determination of CD spectra of porphyrin J – aggregates solid – state samples," Phys. Status Solidi A **205**(4), 797–801 (2008).

29. J. Schellman and H. P. Jensen, "Optical spectroscopy of oriented molecules," Chem. Rev. **87**(6), 1359–1399 (1987).

30. Y. Shimotsuma, S. Kubota, A. Murata, T. Kurita, M. Sakakura, K. Miura, M. Lancry, and B. Poumellec, "Tunability of form birefringence induced by femtosecond laser irradiation in anion – doped silica glass," J. Am. Ceram. Soc. **100**(9), 3912–3919 (2017).

31. S. H. Yoo, R. Ossikovski, and E. Garcia-Caurel, "Experimental study of thickness dependence of polarization and depolarization properties of anisotropic turbid media using Mueller matrix polarimetry and differential decomposition," Appl. Surf. Sci. **421**, 870–877 (2017).

32. A. Champion, M. Beresna, P. Kazansky, and Y. Bellouard, "Stress distribution around femtosecond laser affected zones: effect of nanogratings orientation," Opt. Express **21**(21), 24942–24951 (2013).

33. A. Champion and Y. Bellouard, "Direct volume variation measurements in fused silica specimens exposed to femtosecond laser," Opt. Mater. Express **2**(6), 789–798 (2012).

34. M. Beresna, M. Gecevičius, M. Lancry, B. Poumellec, and P. Kazansky, "Broadband anisotropy of femtosecond laser induced nanogratings in fused silica," Appl. Phys. Lett. **103**(13), 131903 (2013).

35. P. Yeh, "A new optical model for wire grid polarizers," Opt. Commun. **26**(3), 289–292 (1978).

36. S. Ermakov, A. Beletskii, O. Eismont, and V. Nikolaev, "Brief review of liquid crystals," in *Liquid Crystals in Biotribology* (Springer, 2016), pp. 37–56.

37. A. Burneau and C. Carteret, "Near infrared and ab initio study of the vibrational modes of isolated silanol on silica," Phys. Chem. Chem. Phys. **2**(14), 3217–3226 (2000).

38. V. G. Plotnichenko, V. O. Sokolov, and E. M. Dianov, "Hydroxyl groups in high-purity silica glass," J. Non-Cryst. Solids **261**(1-3), 186–194 (2000).